INVESTIGATION OF PERMEABILITY ANOMALIES

Andrew Cable[1], Mike Burke[2]

[1]Weatherford Laboratories UK Limited, Dorset Green Technology Park, Dorset, DT2 8ZB, UK
[2] Wintershall Norge ASA, Kanalpiren, Hinna Park, Laberget 28, NO 4020 Stavanger, Norway

This paper was prepared for presentation at the International Symposium of the Society of Core Analysts held in Austin, Texas, USA 18-21 September, 2011

ABSTRACT

Measured relative permeability curves may be used directly as input data to represent microscopic sweep efficiency in full field simulation models. Imbibition relative permeability, in laboratory units, is effective permeability normalised to some reference permeability (usually effective oil or gas permeability at the irreducible brine saturation, S_{wi}). This paper identifies two types of permeability anomaly observed during measurement processes and their influence on measured relative permeability. The first type of anomaly is where absolute permeabilities differ between phases. We have found that this permeability anomaly is most obvious between brine and gas, but is also observed between oil and brine and is usually associated with a presence of filamentous illite within the rock matrix. This type of abnormal behaviour has been published previously and this paper briefly reviews published literature. The second type of anomaly is a "lubrication effect" due to strong wetting preferences. This too has been published, although we have only found one author, and this paper is reviewed. The aim of this paper is two-fold: (1) to raise awareness so that appropriate reference permeability may be used to normalise relative permeability curves for field simulation models, and (2) to encourage providers of SCAL data to report such permeability 'anomalies' to their clients so that unusual displacement mechanisms can be better understood. In this paper we offer a simple pore scale model and physics that add insight and plausibility into observed permeability phenomena.

INTRODUCTION

Samples for core analysis generally arrive at laboratories as preserved whole core sections. Gamma-ray spectroscopy is generally measured and materials are 'slabbed' for petrographic examination. Routine plugging will take place at intervals specified by the client and sometime preserved whole core sections (30cm lengths) may be set aside for future, more advanced measurement programmes such as capillary pressure, electrical resitivity measurements and relative permeability.

Special core analysis ('SCAL') programmes usually follow routine core analysis (air permeability, helium porosity and grain density measurement). Routine analysis may be supplemented with mercury injection capillary pressure (and pore size distribution), thin section analysis, scanning electron microscopy (SEM) and x-ray diffraction (XRD) in order to provide reservoir geological description and rock typing. It is quite common therefore that SCAL may be undertaken on small core plugs (3.8cm diameter with 5cm length) and start dry (100% gas saturated). If clays are known to be present in samples,

humidity or critical point drying processes may be employed instead of routine hot oven drying. The observation of erroneous permeability data can in most cases be ascribed to the process and saturation history of the sample.

PERMEABILITY MEASUREMENT

Air Permeability

The most common measurement of permeability is air permeability conducted as part of routine core analysis using a proprietary permeameter. Air permeability is an absolute measurement (100% gas saturated) conducted at low pressure (typically 1 bara to 2 bara). Because the measurement is an 'atmospheric' measurement, correction is required for gas slippage (non-zero velocity at the pore walls) usually applied analytically using Klinkenberg correction tables (given inverse mean pore pressure). Not much attention is given to gas flow rate, but this should be constrained to the Darcy flow regime (laminar flow) by the flow meters fitted to the permeameter. A more rigorous (but slightly more time consuming) approach is to measure Klinkenberg permeability (K_L). This involves the measurement of gas permeability at a range of mean pore pressures and plotting permeability versus $1/P_{mean}$. Extrapolation of this data to the ordinate defines K_L and represents the theoretical 'liquid' permeability at infinite pore pressure (laboratories usually provide K_L and $1/P_{mean}$). Klinkenberg published his work in 1941 [1]. Klinkenberg correction is not required where gas measurements are conducted at high pressure (above 15 bara) where gas compressibility can mostly be ignored.

Absolute (Liquid) Permeability

Special core analysis programmes may begin by saturating the dry plug with synthetic formation brine. Absolute brine permeability (K_w) may be measured and data cross-plotted against routine air permeability and porosity data. This very simple process alone will identify many outlying data and apparent 'bad' data. At this stage, process and saturation history of the sample are well understood and so are the pitfalls that may result in bad data, for example:

- Was the sample 100% saturated with air and 100% saturated with brine? An obvious enough question, but for some samples (e.g. low permeability) the routine cleaning process employed using Soxhlet apparatus might be inadequate. Flow through cleaning of samples may be required to ensure that 100% of the pore space is swept clean and saturated.
- To ensure that prepared samples remain 100% brine saturated, samples should be flooded at elevated pressure (>15 bara) for all permeability measurements.
- Measurement of permeability is best achieved by a multi-flow rate process. The measurement of slope (dP/dq) may be used directly in Darcy's equation and eliminates instrument dP off-set. To plot transient data and use linear regression analysis will provide the standard measurement error and 'goodness'of fit of the raw data (which may run into hundreds, or thousands, of data points when logging live time (see Figure 1).

- For high permeability samples (>300mD-500mD) measurement of differential pressure is required directly across the core plug end-faces (since pressure loss in 1/8th inch tubing is not insignificant compared to pressure loss across the core sample).
- Assuming that the geometry of the sample is adequately described (length and diameter), sample is cleaned, fully saturated and permeability is measured rigourously as described, the main measurement uncertainty is ascribed to fluid viscosity which should be measured for a range of laboratory temperatures.

Effective Permeability

Effective permeability, otherwise known as 'end-points' are two phase permeability measurements where one of the phases is (assumed) immobile. So for our brine saturated sample a primary drainage process is required to establish an irreducible brine saturation (S_{wi}). The drainage process might be achieved by: (1) core flooding, (2) centrifuge or (3) porous plate which may in turn use oil (refined laboratory oil or stock tank oil) or gas as the injected phase and often integrated with other measurements (for example multi-speed centrifuge capillary pressure or porous plate combined with electrical measurements for saturation exponent). Effective oil (or gas) permeability (k_e) at this stage is measured using cleaned state core. For effective oil permeability (k_{eo}) it may also be measured after wettability restoration, known as restored state.

At this point in the laboratory process the saturation history is well understood from a knowledge of brine production(s) and the pore volume of the sample (determined from routine core analysis). If using multi-stage processes, for example for the derivation of capillary pressure curves and saturation exponent, it might be desirable to perform a saturation QC (quality control). This may be in the form of an extraction process e.g. Dean & Stark, Karl Fischer titration, tracer analyses or directly with γ-ray insitu saturation monitoring.

End point permeability may also be measured after an imbibition process (following wettability restoration) to derive effective brine permeability (k_{ew}) at residual oil saturation (S_{or}). This data is usually normalised against effective oil permeability (k_{eo}) at S_{wi} to define relative permeability, both k_{rw} and k_{ro} curves. Analytical techniques, such as JBN analysis, or core flood simulation tools too would use effective oil permeability for the derivation of relative permeability curves.

Native State (Effective) Permeability

Samples cut from whole preserved core may be used for permeability measurement in their native state (uncleaned). To use native samples is to accept some higher degree of saturation uncertainty and an uncertainty of sample wettability. The preserved core may have been cut with water-based and/or oil based drilling muds. The samples may show evidence of mud invasion and may exhibit an overly oil-wetting character, either by contact with oil based mud or simply by raising the samples to surface conditions with insitu oil in place. But none-the-less permeability data prior to solvent cleaning (and drying) can be very useful.

Native samples may be flooded (or centrifuged) using synthetic formation brine. Measurement of effective (brine) permeability, after brine flushing at elevated pressure to both 'clean' and degas the sample, may give an indication of brine permeability at residual oil saturation (S_{or}). Similarly, the sample may be flooded with 'oil' to measure oil permeability at native S_{wi}. This may be quite useful if it is not possible to establish reservoir S_{wi} using cleaned state samples (because cleaned samples are both water-wetting and may have high capillary pressure). The choice of oil is also important since direct contact of reservoir oil with a refined laboratory oil may cause asphaltene deposition and permeability loss due to pore blocking. The use of a depolar dekalin 'slug' prior to using the laboratory oil should avoid this issue.

EXAMPLES OF OBSERVED ANOMALIES

The general expectation is that absolute permeability is absolute and that it should be the highest value for the rock sample. And nor should absolute permeability depend on the fluid used to make the measurement.

Permeability variation might be expected when working with high permeability and/or poorly consolidated samples. The application of net overburden pressure on the core sleeve will affect permeability, with both permanent and reversible deformation of the sample. Permeability variation attributable to variable overburden stress, fines migration in excess of critical flow velocity, sample grain loss, pore blocking from fluid interactions or material displacement are not presented in this paper. This paper seeks to unravel genuine permeability anomalies and apply fluid mechanics to offer flow scenarios that fit the observations.

Low Gas Permeability (Non-Darcy Flow)

It is possible to observe absolute gas permeability data that are significantly lower in value than measured absolute brine permeability on the same samples. When the authors have observed such data, it can be reconciled by assuming non-Darcy flow regime and using the analysis of Evans et al. [2]. Forcheimer [3] suggested in 1930 that the resistance to flow should be considered in two parts: resistance due to viscous drag and losses due to turbulent eddies resulting from changes in the cross section of the channels. At low rates of flow viscous drag (skin friction) will predominate but at higher rates of flow and in very thin beds where enlargement and contraction losses become significant turbulent eddies will predominate. At very high flow rates viscous forces are negligible, see equation 4.15 [4]. Calculation of permeability in non-Darcy flowing conditions is conveniently summarised in reference [5].

Low Brine Permeability (Permeability Loss)

Observation of (unexpected) low absolute brine permeability may be an indication of permeability loss resulting from laboratory processes and therefore an artefact. There are two processes to consider since the lower than expected brine permeability could be a result of reference to an (incorrect) absolute gas (air) permeability measurement after sample drying, but equally could be referenced to native permeability. There are reports in the literature where low brine permeability, relative to gas permeability, is ascribed to clay such as filamentous illite [6, 7]. It is the presence of 'wispy' illitic extensions (see

Figure 2) that is most probably responsible for the observed absolute permeability changes. It is not difficult to envisage that clay shrinkage may occur when the core exists in the gas phase (the fibrous material may collapse when dry) and clay swelling occurs in the brine phase. The fibrous illitic clay when swollen (saturated) may reduce or turn off flow channels when flowing the brine phase as the clay extensions may block pore throat locations. Reference [7] is recommended for further reading here since this report contains a literature survey (2004) and many additional references. It should be noted that for single phase brine (or gas) permeability measurement the fluid is in direct contact with the rock (surface roughness).

The second process is absolute brine permeability relative to native permeability measurement. Native permeability might be an effective brine permeability (at S_{or}) and/or an effective oil permeability (at S_{wr}). The authors have measurement data (which remain unpublished) where native brine permeability may be measured on samples 200mD-600mD only to measure absolute brine permeability of 5mD–150mD (40 to 4-fold reduction in permeability). SEM and petrographic description show widespread grain coating clay and pores filled with detrital clay. Pore-filling kaolinite that is marginally replaced by illite and quartz overgrowth that has overgrown with grain-coating detrital clay. Illite platelets have wispy authigenic overgrowths. Here the cleaning process used to establish 100% brine saturation (65kppm) was a mild miscible flow-through process using cold toluene and methanol cycles without drying processes. A loss in sample absolute permeability does not necessarily affect relative permeability (curves) when using an effective oil permeability reference.

Oil Relative Permeability>1

The first example is effective permeability measured at immobile brine saturation (S_{wi}) which is greater than absolute permeability. It is best to consider the case of effective oil permeability (k_{eo}) higher than absolute brine permeability (K_w). There are good examples of effective gas permeability (k_{eg}) higher than absolute gas or brine permeability (K_g or K_w) [7], but these scenarios are possibly further complicated by clay swelling issues as discussed. For the case given for oil-water, the measurement follows a primary drainage process using cleaned core, so the rock surface is deemed to be ‘water-wetting’ and the flowing medium (oil) would be the non-wetting phase.

A good overview of the effects of strong wetting on relative permeability for oil-wet carbonates (with matched viscosity ratio) is given by McPhee [8]. This reference drew attention to ‘lubricated flow' where a non-wetting flowing phase is lubricated by a (static) wetting phase.

For our example, in the case of a strongly water wet core at irreducible brine saturation (S_{wi}), the brine will occupy all of the smaller pores and will wet all of the rock surfaces. This wetting effectively isolates the flowing phase (oil) from the rough rock surfaces, thus easing the flow (of oil). The mechanism assumes that there is much less drag between the non-wetting phase and wetting phase interface than between the wetting phase and rock surfaces. If this is the case, measured effective permeability may well be higher than the measured absolute permeability.

An inter-laboratory comparison of SCAL data published in 1994 [9] supported the observation that oil relative permeability (k_{ro}) measured at S_{wi} could be greater than unity. This paper was a comparative study between four service contractors; but made some important references to abnormal permeability behaviour. The study used Clashach (outcrop sandstone) as the 'test' rock which was known to contain around 2% illite. Plugs were cut and conventionally cleaned and dried. The authors expected plugs to be desaturated to an immobile brine saturation of around 0.08 frac. The controlling laboratory and one service provider reported effective oil permeability relative to the absolute brine permeability in excess of unity (1.01 to 1.47).

For this paper the authors can cite many examples where k_{eo} measured at S_{wi} is higher than absolute brine permeability. Most data remain the property of sponsoring clients and data are not available for publication. A recent centrifuge study, summarised by Table 1, revealed all six plugs under test to have oil relative permeability in excess of unity (values observed from 1.03 to 1.26). This feature in the measurement data is not specific to a laboratory centrifuge process, short samples nor specific to the very low immobile brine saturations achieved. Recent (unpublished) data using porous plate method and with the aid of insitu saturation monitoring to establish S_{wi} circa 0.15 frac. gave oil relative permeability in excess of unity ranging from 1.05 to 1.18.

Brine Relative Permeability>1

The second example is effective brine permeability (k_{ew}) measured at residual oil saturation (S_{or}). This data is usually normalised against effective oil permeability (k_{eo}) at S_{wi} to define relative permeability curves. When k_{rw} is observed greater than unity, data is usually treated which such scepticism it is disqualified. The measurements presented in Table 2 are recent centrifuge imbibition k_{ro} data which may be disqualified due to the unusual end-point data. It is this k_{rw} data greater than unity that has inspired the pore modelling and flow mechanics presented in the next section, but it is equally relevant to observation of k_{ro} greater than unity (at S_{wi}).

Post Experiment Absolute Permeability

After relative permeability measurement programmes it is a simple matter to measure 100% brine (K_w) and 100% oil absolute permeability (K_o). When using insitu saturation monitoring to quantify transient saturation data 100% phase calibrations are required in any case. We have seen examples where K_w is 40% of the value of K_o, but equally examples where $K_w>K_o$. Ideally, the 100% phase permeabilities (including gas) are all quite similar.

FLOW MECHANICS

In porous media tortuosity is both complex and variable. Tortuosity exist as pore size distribution with varying pore-pore throat diameter. The rock matrix is both varied in mineralogy, grain coatings, cementation components (clays for example) embedded inclusions, vugs and fractures (see Figure 2). Mineralogical tortuosity might be considered 'fixed', but tortuosity may be further altered by fluid distributions. For example wetting fluids will spread over certain minerals. Residual fluid (immobile saturation) may both wet minerals as a 'boundary layer' and occupy surface asperities

('corners'). Some fluid may also change the 'fixed' tortuosity of the sample. For example brine (and gas) interaction with clay causing the clay mineral to swell (and shrink). These changes have profound implication for fluid dynamics.

Fluid flow friction in pipes and channels is a very mature science, most are familiar with Bernoulli's equation to describe momentum changes in fluid. Reynolds in 1883 established that flow will vary with velocity, physical properties of the fluid and the geometry of the surface. Pressure gradient in flow attributable to laminar flow, turbulent flow, surface roughness, tortuosity and boundary layer effects are well understood and published. A good overview is given by Coulson & Richardson [10].

Some Physics of Geometry Related Forces

Deposits of S_{or} in porous medium will generally lead to a reduction in effective porosity, defined here as porosity contributing to the effective flow area and intuitively this will always result in $k_{rw}<1$. However, speculation is made that pore geometry can result in counter intuitive measurements, whereby $k_{rw}>1$, and as a first step towards understanding the plausibility of such measurements a description of three geometry related forces acting on brine flowing through a pore is given.

1…Drag or Friction. Drag forces are assumed to be linearly proportional to the brine velocity and inversely proportional to the effective flow area. For a small interval Δx the drag force is obtained as $\Delta F_{drag}=(KV/A_{pore})\Delta x$ and considering $V=V_{throat}A_{throat}/A_{pore}$ the total drag force becomes $F_{drag}=\Sigma(KV_{throat}A_{throat}/A_{pore}^2)\Delta x$, whereby the constant $KV_{throat}A_{throat}$ is here labelled "drag coefficient". Figure 3 plots the relative drag force against the pore and throat effective area ratio and shows that for decreasing pore size this force always increases. In other words the drag force *never* acts to increase permeability as effective porosity decreases.

2…Collision. A second force is introduced to quantify the effect of brine collision with the pore face, or any other obstructing feature, prior to exiting at the pore throat. The incremental collision force ΔF caused by the impact of brine on a small section Δy can be calculated as $\Delta F_x=(\rho V^2(1-\cos\theta))\Delta y$ and $\Delta F_y=(\rho V^2\sin\theta)\Delta y$; whereby ρ is the density of brine and θ the slope of the colliding interface. Generally θ will be a function of y, for example a curved function related to the contact angle may be preferable if deposits of S_{or} form the colliding face. The incremental force ΔF_y acts orthogonal to the flow direction and away from the colliding face while ΔF_x acts parallel and against the flow direction. For the purpose of calculating flow resistance only ΔF_x is considered and summation across the obstructing face yields $F_{collision}=\Sigma(\rho(V_{throat}A_{throat}/A_{pore})^2*(1-\cos\theta))\Delta y$. Assuming a 90° colliding face the relative $F_{collision}$ is calculated for various pore/throat effective area ratios and plotted in Figure 3. This shows that for pore to throat effective area ratios less than 2 the resistance to flow will decrease as relative pore size decreases: That is the collision force *sometimes* acts to increase permeability as effective porosity decreases.

3…Change in Momentum. The kinetic energy of a brine control volume of unit mass in the pore body is given by $Ke_{pore}=\frac{1}{2}V_{pore}^2$, and that of the same control volume in the pore throat by $Ke_{throat}=\frac{1}{2}V_{throat}^2$. As $V_{throat}>V_{pore}$ an amount of energy equal to $\frac{1}{2}(V_{throat}^2-$

V_{pore}^2) is lost to heat when passing from the entrance pore throat to pore body. On passing from pore body to exit pore throat the original energy state is restored as the brine returns to the velocity V_{throat}. This change in velocity requires a force, $F_{momentum}$, which is proportional to the change in velocity V_{throat}-V_{pore}. Figure 3 plots the relative $F_{momentum}$ with respect to the pore to throat effective area ratio and reveals a second counter intuitive result: The force due to brine momentum changes *always* acts to increase permeability as effective porosity decreases.

A Pore Model Using Drag and Collision Forces

While the above discussion indicates k_{rw}>1 can, in theory, be a correct measurement, without knowing the magnitude of the various forces involved we cannot judge if such results are actually plausible, or just theoretically possible. Therefore, in a spirit of enquiry and with limited time and facilities available, a simple simulation of how k_{rw} would change as pore geometry is varied by S_{or} presence was undertaken.

In building the model the following assumptions and approximations have been made: 1) S_{or} volumes are calculated using a cuboid pore with entrance and exit throats in the middle of opposite faces - see Figure 4. It should be noted that this volume only concerns the portion of S_{or} which could lead to k_{rw}>1 (by reducing the collision force) and unquestionably results in an underestimation of what would actually be measured as S_{or}. 2) S_{or} is placed evenly along the 12 cuboid line-angles and it is assumed that these are the only volumes where S_{or} is found. 3) As time limitations restricted any investigation of curved surfaces both the S_{or} interface and the pore face are assumed straight. 4) For collision calculations the cuboid pore was converted to a tubular pore whereby the tubular effective flow area at each cross-section is equal to that of the cuboid. 5) For the tubular pore a laminar Poiseuille flow profile was used. 6) Drag and collision forces are calculated as above and no consideration is given to forces resulting from brine momentum changes. 7) No consideration is given to transients or entrance length effects.

The steps undertaken to achieve the model were: 1) Calculate the volume of S_{or} along all 12 cuboid line-angles and divide by the total cuboid pore volume to obtain S_{or}. 2) Change to an equivalent tube shaped pore by calculating the geometry of an equivalent circle for each cuboid pore cross-section. 3) Assume Poiseuille laminar flow and calculate the relative mean velocities and flow profiles for each cross-section. 4) Calculate the drag and collision forces at each cross-section. 5) Take the inverse of the sum of the drag and collision forces as representing brine permeability with S_{or}. 6) Take the ratio of this permeability with respect to that calculated where no S_{or} is present and assume this is represents k_{rw}. 7) Plot k_{rw} versus S_{or}. In the model the following parameters can be changed. 1) Slope angle of the S_{or} interface and pore exit face - see Figure 5. 2) The ratio of the effective throat to pore flow area (calculated without S_{or}). 3) The amount of S_{or}. 4) The drag coefficient.

With reference to Figures 4&5, for each cross-section where the effective flow area changes a summary of the resultant force calculations is given. 1) *Flow at entrance pore throat (no S_{or}).* The mean velocity of laminar flow profile brine decreases in a step function. No forces are calculated. 2) *Flow at entrance pore throat (with S_{or}).* Drag

forces are calculated at the sloped interface using a changing mean velocity derived in accordance with the reduction in effective flow area arising from S_{or} deposits along the 4 line-angles framing the entrance throat face. 3) *Flow through the main pore body (with and without S_{or}).* Drag forces are calculated with and without S_{or} along the 4 line-angles at the top and bottom of the pore. 4) *Flow directly through exit pore throat (with and without S_{or}).* The mean velocity of laminar flow profile brine increases in a step function. No forces are calculated. 5) *Collision with pore face framing the exit throat (no S_{or}).* Collision forces are calculated for laminar flow colliding with the effective flow area of the circular exit throat frame of the remaining pore face. 6) *Drag forces through S_{or} sloped interface at exit throat (S_{or} present).* Drag forces are calculated at the sloped interface using a changing mean velocity calculated in accordance with the reduction in effective flow area arising from S_{or} deposits along the 4 line-angles framing the exit throat face. 7) *Collision forces with S_{or} sloped interface at exit throat (S_{or} present).* Primary collision forces are calculated using a laminar flow profile based on the geometry of the main pore body but using an increased mean velocity calculated in accordance with the reduction in effective flow area arising from S_{or} deposits along the 4 line-angles framing the exit throat face. Collision rotates the flow by the angle equal to that of the S_{or} interface and then moves move parallel to the interface slope. This flow moving parallel to the S_{or} interface experiences a second collision with the pore face and secondary collision forces are calculated at an angle corresponding to the difference between the S_{or} interface and pore face. 8) *Collision forces with pore face at exit throat (S_{or} present).* Collision forces are calculated using a laminar flow profile based on the geometry of the main pore body but using an increased mean velocity calculated in accordance with the reduction in effective flow area arising from S_{or} deposits along the 4 line-angles framing the exit throat face.

Results: Using the numerical model with slopes of 45° for the S_{or} interface and 90° for the pore face, the following investigations were undertaken: 1) *Variance of k_{rw} with drag coefficient.* Figure 6 presents the variation of maximum k_{rw} versus the base pore to throat effective area ratio (calculated without S_{or}) with a varying drag coefficient. It shows the variance of k_{rw} to be relatively small for large changes in drag coefficient and based on this insensitivity a coefficient of 1 is taken as default. 2) *Variance of k_{rw} with S_{or} for varying base pore to throat effective area ratios.* The results are shown in Figures 7a&7b and reveal: 2a) A maximum k_{rw} of 1.32 is calculated at an S_{or} of 0.5% and an effective area ratio of 1.13 (corresponding to a relatively small "step" into the pore throat of around 6% of pore height). 2b) k_{rw} is always above 1 for S_{or} less than 3.5% and always less than 1 for S_{or} greater than 3.5%. Note that the method of S_{or} calculation (see above) should be considered when judging the reasonableness of these S_{or} values. 2c) For base pore to throat effective area ratios less than 1.29 (corresponding to a "step" of 12% of pore height) the maximum k_{rw} is achieved when S_{or} reaches the top of the step; in other words the step has been completely smoothed by S_{or}. 2d) Where "step" height is greater than 12% the maximum k_{rw} is achieved when S_{or} has reached some intermediate distance up the pore face.

Pore Modelling Conclusion: While the reader is left to judge the validity of this simple approach to estimating k_{rw}, the results of the numerical model indicate that pore geometry combined with S_{or} can plausibly cause k_{rw} >1. The model further indicates this effect to be more pronounced where the dimensions of pore body and throat are so similar that they are more accurately described as one uneven pore.

CONCLUSIONS

Laboratory measurements and pore modelling show that it is quite plausible to have end point relative permeability data in excess of unity. Such data should not necessarily be disqualified if measurement protocols are adhered too and there are no obvious reason for data exclusion. In fact more measurement data should be sought, for example 100% brine (K_w), 100% oil absolute permeability (K_o) SEM and mineraology to gain further insights. Ideally, the 100% phase permeabilities (including gas) should be quite similar (identical), but more often is the case that they are not. The laboratory relative permeability data will usually be normalised to k_{eo} @ S_{wi}, for an imbibition process (e.g. water displacing oil or brine displacing gas). For a drainage process (e.g. gas displacing oil, or oil displacing brine) the laboratory might normalise data to an absolute pemeability.

For field simulation, for example when modelling using Eclipse, a relative permeability input table is required. Eclipse does not require any of the endpoints to be equal to 1, it will simply take relative permeability from the lookup table for a given block water saturation. Eclipse will multiple that number by the defined block permeability. So it does not matter if relative permeability is normalised to K_{air}, K_L (Klinkenberg corrected gas permeability) or k_{eo} @ S_{wi} providing that the block permeability is appropriately defined.

ACKNOWLEDGEMENTS

The authors would like to thank DECC (UK Department of Energy and Climate Change) for allowing reference [7] to be entered into the public domain.

REFERENCES

[1] Klinkenberg, L. J. “The permeability of porous media to liquids and gases” Drilling and Production Practice, 1941, American Petroleum Inst., pp. 200–213.

[2] Evans, R.D. et al “The Effect of an Immobile Liquid Saturation on the Non-Darcy Flow Coefficient in Porous Media,” SPE Prod Eng, November 1987, p331-338.

[3] Forcheimer, P. “Hydraulic” Teubner 1930.

[4] Coulson, Richardson with Backhurst and Harker “Chemical Engineering Volume Two” Pergamon Press Third Edition, 1980.

[5] Mott, R.E., A.S. Cable and M.C. Spearing “Measurements and Simulation of Inertial and High Capillary Number Flow Phenomena in Gas-Condensate Relative Permeability” SPE62932 Annual Technical Conference and Exhibition held in Dallas, Texas, 1-4 October 2000.

[6] Mikkelsen, M., A. Scheie, O.Rong and E.T. Boer “Abnormal Permeability Behaviour of a North Sea Sandstone Reservoir” SPE 22600 Dallas Texas October 6-9, 1991.

[7] Cable, A.S. "Investigation of Reference Permeability Anomalies" (May 2004, published February 2011 at http://www.og-mrp.com/dissemination/relperm/misc/Ref_Perm_Anom_v1.pdf).
[8] McPhee, C.A. "Effect of Strong Wetting on End-point Relative Permeability" Edinburgh Petroleum Services Ltd. Dialog July 1994.
[9] McPhee, C.A. and K.G.Arthur "Relative Permeability Measurements: An Inter-Laboratory Comparison" SPE 28826 October 25-27 1994.
[10] Coulson, Richardson with Backhurst and Harker "Chemical Engineering Volume One" Pergamon Press Third Edition, 1980.

Table 1. Recent Example of Anomalous Permeability Data ($k_{ro} > 1$)

Sample ID	**3-2**	**4-1**	**4-2**	**9-2**	**10-2**	**11-2**
Length (cm)	4.984	4.781	4.873	4.893	4.889	4.896
Diameter (cm)	3.796	3.796	3.796	3.796	3.796	3.795
Basic Properties						
K_{air} -Klinkenberg corrected (mD)	143	236	213	273	156	184
K_w (mD) - Absolute Brine	88	145	138	242	144	142
K_{air}/K_w	1.6	1.6	1.5	1.1	1.1	1.3
Drainage						
S_{wi} (frac.)	0.03	0.01	0.04	0.02	0.02	0.02
k_{eo} (S_{wi}) (mD)	98	155	174	260	149	166
$k_{eo}(S_{wi})/K_w$ - k_{ro}	1.12	1.07	1.26	1.07	1.03	1.17

Table 2. Recent Example of Anomalous Permeability Data ($k_{rw} > 1$)

Sample ID	**3-2**	**4-1**	**4-2**	**8-2**	**9-1**	**11-2**
Imbibition						
S_w (frac.)	0.854	0.881	0.894	0.849	0.856	0.789
S_{or} (frac.)	0.146	0.119	0.106	0.151	0.144	0.211
k_w @ S_{or} (mD)	102	170	158	485	505	152
k_{rw}	1.02	1.28	1.11	1.13	1.08	0.97

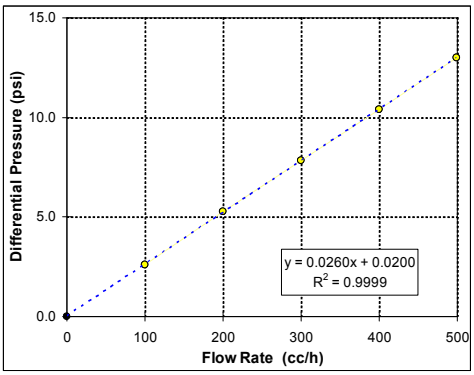

FIGURE 1: kw Measurement at S_{or}

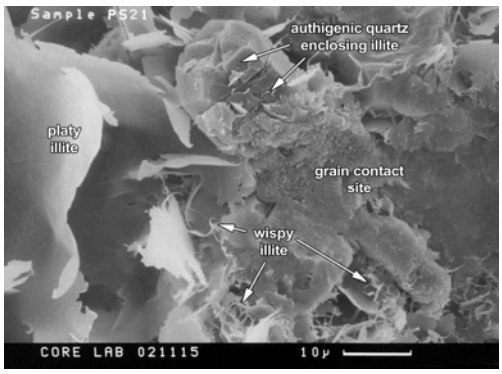

FIGURE 2: Pore Structure with Clay

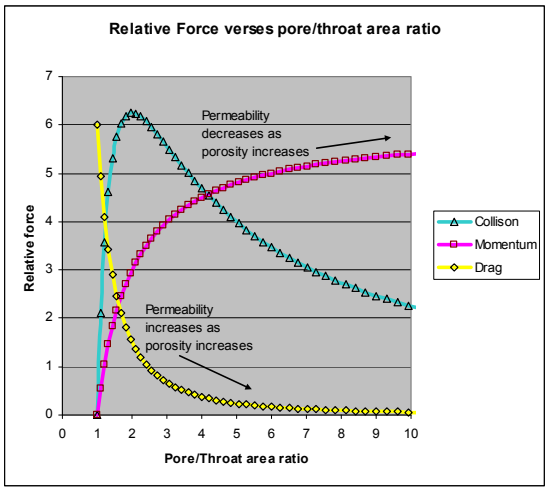

Figure 3: Force Summary

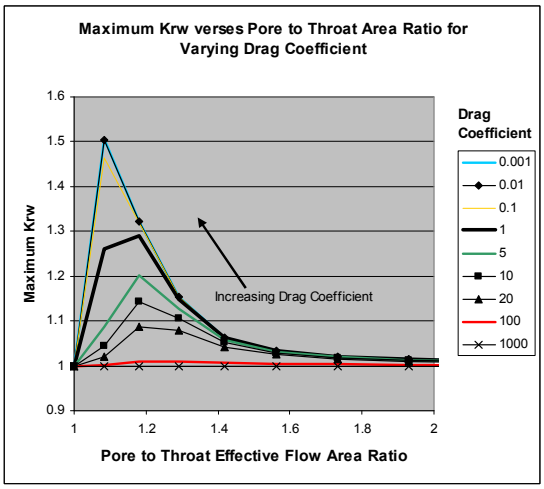

Figure 6: Drag Coefficient Variation

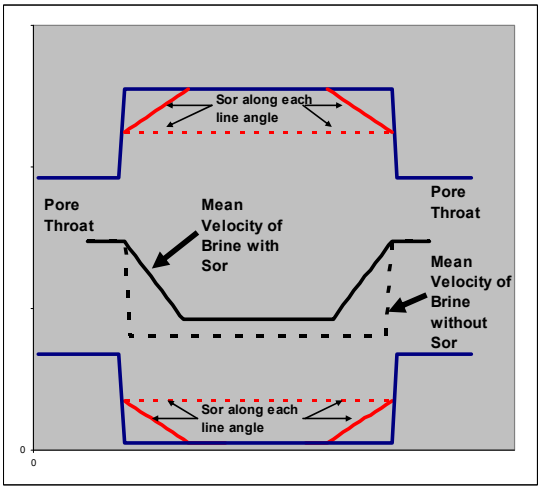

Figure 4: Synthetic Pore Schematic

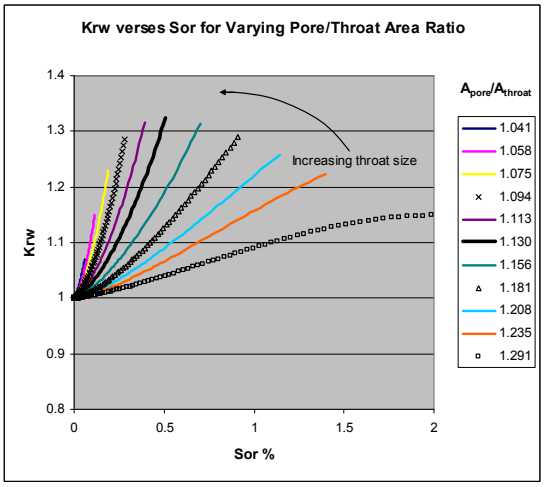

Figure 7a: K_{rw} verses S_{or}

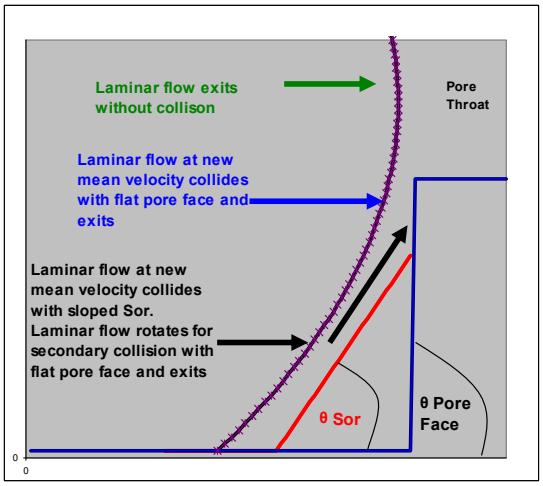

Figure 5: Collision Schematic

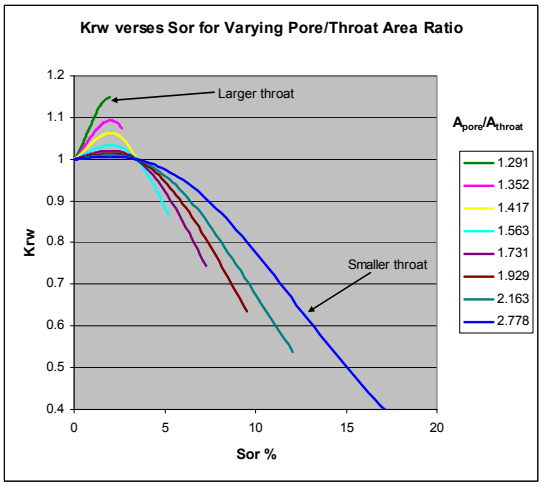

Figure 7b: K_{rw} verses S_{or}